PARTICLE MIGRATION IN A HELLE–SHAW CELL WITH NON-PARALLEL WALLS

Jana WICHTERLOVA[1], Ondrej WEIN[2,*] and Frantisek KASTANEK[3]

Institute of Chemical Process Fundamentals, Academy of Sciences of the Czech Republic, 165 02 Prague 6-Suchdol, Czech Republic; e-mail: [1] wih47@vsb.cz, [2] webox@icpf.cas.cz, [3] kastanek@icpf.cas.cz

Received December 22, 1997
Accepted February 14, 1998

Motion of a single macroscopic particle in a liquid flowing through a narrow channel with slightly non-parallel walls is studied by a visualization method. The experiment is limited to the region of slight inertia effects, $Ar < 500$. Three kinematic characteristics of the particle motion in the channel, *viz*. settling velocity in a still liquid, as well as longitudinal and lateral migration velocities under non-zero flow, are determined and correlated in dependence on the operation parameters. Both the longitudinal characteristics strongly depend on the particle-to-channel size ratio and are only slightly affected by inertia effects. On the other hand, the inertia effects play an essential role in the mechanism of lateral migration.

Key words: Helle–Shaw cell; Sedimentation; Longitudinal migration; Lateral migration.

Relative motion of a particle in liquid, still or flowing, with or without gravity or other body force effect is a subject both of pragmatic (separation operations, multiphase flows, physiology) and theoretical interest. Recent computer studies of the liquid–particle–wall non-linear interactions[1,2] indicate that an *a priori* estimate of the order-of-magnitude of the effects of basic parameters (particle and flow Reynolds numbers, geometric simplexes) is needed for a reasonable simplification of the starting Navier–Stokes equations. It seems that some new experimental impulses are needed for the further development of this branch of computational hydrodynamics.

Besides the classic sedimentation of small particles in large vessels, most of low-*Re* experiments are focused on radial migration of a sphere in the Poiseuille flow towards a critical radius[3]. Even here, only few studies provide a quantitative estimate of the migration velocities[4].

We present here a visualization experiment displaying rather remarkable and easily observable lateral migration. An unbalanced rigid spherical particle moves in the verti-

* The author to whom correspondence should be addressed.

cal flow of a Newtonian liquid through a vertical Helle–Shaw cell (narrow channel of a constant cross-section for the flow visualization from the front view) with slightly non-parallel walls. Liquid/particle densities are chosen in such a way that the particle tends to move in the direction opposite to that of the liquid flow. As a result, the particle residence time in the channel is long enough to observe an apparent lateral migration. The flow regime is controlled by only a few parameters and the flow patterns are relatively simple. This gives an opportunity to compare, in future, the observed particle kinematics with a theoretical prediction.

EXPERIMENTAL

Apparatus and Measurements

The experimental set-up, shown in Fig. 1, consists of the vertical narrow channel with a transparent wall for visual observations from the front view (the Helle–Shaw cell), the facilities for liquid circulation through the channel, and the visualization/recording system. The front and back walls are slightly non-parallel and create a narrow vertical channel of constant trapezoidal cross-section. The verticality is carefully adjusted before each series of experimental runs.

TABLE I
Channel geometries used

Channel	W mm	h_0 mm	h_1 mm	tg α
S	140	2.9	9.7	0.049
M	140	2.9	14.2	0.081
L	140	5.6	18.4	0.091

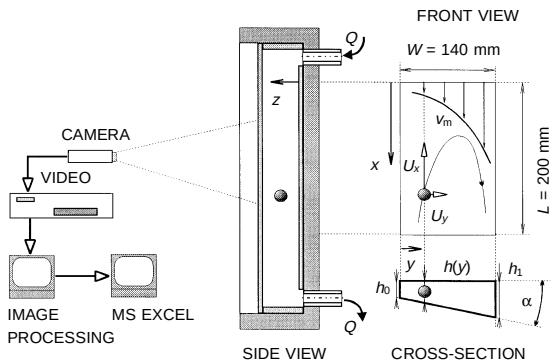

FIG. 1
Experimental set-up

A highly viscous Newtonian working liquid is pumped downwards through the channel with a constant flow rate Q from a free-surface receiver with foam breakers by a helical-screw pump. The sides of the channel are of unequal depths h_0 and h_1, adjustable by replacing the pair of trapezoidal spacers, on which the transparent front wall is fixed by a special sealing. The total height of the channel is 500 mm. Various cross-sections are listed in Table I. Honeycombs are placed in both inlet and outlet sections inside the channel, with the aim to reduce the regions of undeveloped channel flow (not monitored by a TV camera) to the extent of approximately 150 mm. The region of fully developed channel flow with strictly parallel streamlines is checked for each experimental run. A set of streamlines is visualized by injecting a colored tracer liquid from six injection points placed laterally in the channel head. The tracer liquid is prepared by a small amount of a concentrated aqueous solution of both potassium hydroxide and phenolphthalein to a part of the working liquid.

Test particles are rigid buoyant spheres made of commercial plastic beads. Each particle contains a piece of iron wire glued by an epoxy resin inside its axial hole. Prior to each visualization experiment, the particle is fixed by a magnet in an initial position at the front wall. After removing the magnet at a suitable moment, the untied particle is driven by gravity and the liquid stream in the channel. The particle initial position and its motion immediately after the start are shown, from the side view, in Fig. 2. These observations can be actually made because the Perspex sides of the channel are carefully polished. In the experiments with a non-zero flow rate, particles move rapidly toward the channel axis and actually move in the plane of symmetry between the bounding front and back glass walls of the channel. In the settling experiments with a still liquid, $Q = 0$, the particles move too fast and, probably, they are not centered perfectly during the visualization period. Anyway, the visualization measurements are treated under tacit assumption that the particles are spontaneously centered to the plane of channel symmetry. Imperfect centering probably introduces some errors into the treated visualization data.

The particle trajectory, shown in the front-view part of Fig. 1, is recorded by a TV camera/video-recorder on a tape and treated off-line by using an image processing PC package to provide two components U_x, U_y of the local migration velocity. The operation parameters which control the velocity of the particle rise, $U_0 < 0$, and the local maximum of the liquid velocity at a given location (x, y), $v_m > 0$, are chosen in such a way that there is a lateral position where the particle rise (relative to the liquid) and liquid flow interfere, $|1 + U_0/v_m| << 1$, which results in the particle levitation, $U_x \approx 0$. Note that this lateral position corresponds to the return point of the parabolic particle trajectory shown in Fig. 1. With the mentioned choice of operation parameters, the particle residence time in the visualized region is maximized and the lateral migration (in the y-direction) becomes as pronounced as possible.

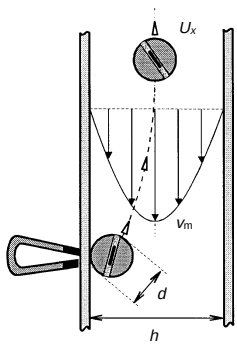

FIG. 2
Start-up process of a test particle, side view

Properties of Particles and Liquids

The volume V and mass m of the test particle are determined by weighing it alone and in a pycnometer. Diameters d and apparent densities ρ_p of the used four particles P1–P4, calculated from the well-known formulas $\rho_p = m/V$, $d = (6V/\pi)^{1/3}$, are given in Table II.

Two highly-concentrated aqueous solutions of glycerol (L1 and L2 containing approximately 15 and 30% of water, respectively) are used as working liquids. Rough estimates of their properties are given in Table II. As the experiments were run under changing ambient temperature (20–25 °C), and the working liquids in the foam breaker were exposed to ambient air with variable humidity, the liquid properties ρ and ν, which depend both on the temperature and water content, were determined every day after finishing the visualization experiments, and corrected for the actual temperature during each run. The intervals of the *Ar* number for each particle–liquid combination, given in Tables II and III, reflect the actual changes of the liquid properties.

Terminal Settling Velocities

Terminal settling velocity U_∞ of a particle in a large volume of the still liquid is a primary quantitative characteristic of this system. In a few preliminary experiments, we found that the calculation of

TABLE II
Basic parameters of the particle–liquid systems used

Particle, liquid	d mm	ρ_p kg m^{-3}	$10^6 . \nu$ m^2 s^{-1}	ρ kg m^{-3}	T °C	*Ar*	$\lvert U_\infty \rvert$ mm s^{-1}
P2, L2	8.18	1 157	15	1 183	21–25	400–500	25–27
P1, L2	6.03	1 148	15	1 183	21–25	200–300	21–23
P2, L1	8.18	1 157	80	1 226	22	45	20
P1, L1	6.03	1 148	80	1 226	20–24	20–30	13–15
P4, L1	5.00	1 142	80	1 226	22	12	10
P3, L1	4.23	1 202	80	1 226	21	2	2

TABLE III
Parameters of the flow experiments

Particle, liquid	*Ar*	Channel	h mm	λ	$-Re_0$	v_m mm s^{-1}	Re_m
P2, L2	400–500	M, L	9–15	0.56–0.93	3.0–7.5	6–38	3.0–30.0
P1, L2	200–300	M, L	7–14	0.42–0.89	3.0–6.0	5–34	3.5–25.0
P2, L1	45	M	9–12	0.70–0.97	0.2–0.9	5–11	0.6–1.6
P1, L1	20–30	S, M, L	7–14	0.43–0.94	0.25–0.8	5–11	0.4–2.3
P4, L1	12	M	7–12	0.43–0.69	0.3–0.4	4–7	0.4–1.0
P3, L1	2	M	7–8	0.54–0.62	0.06	1.1–1.4	0.1

U_∞, based on commonly known formulas and carefully determined basic physical properties of the particles and liquids, provides better results than an improvised sedimentation experiment in available vessels of radii smaller than 100 mm and heights lower than 500 mm where both the wall and start-up effects play a negligible role. The terminal settling velocities were calculated from the primary parameters (through Ar, Re_∞) using the formula

$$U_\infty\, d/\nu \equiv Re_\infty = Ar/[18 + (Ar/2)^{1/2}] \ , \qquad (1)$$

which is, for $Ar < 1\ 000$, an acceptably accurate inversion to the correlation

$$Ar = 18\, Re_\infty(1 + Re_\infty^{1/2}/6 + Re_\infty/60) \ , \qquad (2)$$

proposed in ref.[5].

Visualization and Image Processing

The particle motion in the front view is recorded by a TV camera PULNIX TM-765E on a tape format S-VHS by using a videorecorder MITSUBISHI HS 5600(RS) with speed 23.4 mm s^{-1}. The record is simultaneously monitored on a small TV screen. The chosen distance between the camera and channel guarantees covering the overall region of the well-developed flow and particle motion, approximately 200 mm by height and 150 mm by width (see the front view in Fig. 1). The duration of a single run (*i.e.*, the residence time of the particle inside the visualized area) varies between 10 and 3 000 s (see Table IV).

The visual records were treated by using a common PC equipped with an additional graphical PC-card (a grabber) and a monitor. A simple home-made software makes it possible to move the tape in the videorecorder, to identify interactively the instantaneous particle position on a frame with the accuracy of a single pixel (approximately 0.5 mm in vertical and 0.3 mm in horizontal direction), and to write the results $x_i = x(t_i)$, $y_i = y(t_i)$ into a text file. A calibration procedure for adjusting a correct metrics in the visualized plane, using three or more non-colinear points with known positions, is a part of the software. The obtained primary data on the particle trajectories were treated separately, using the Microsoft Excel solver.

ANALYSIS

Localization of the Sedimentation and Migration Data, Correlation Scheme

The ultimate aim of the present study is to correlate quantitatively the primary data on the particle trajectories in the terms which make it possible – in future – to compare the obtained results with a hydrodynamic theory. This study is limited to narrow channels

TABLE IV
Range of kinematic quantities observed

Process	$\lvert U_x\rvert$ mm s^{-1}	$\lvert U_y\rvert$ mm s^{-1}	t_{res} s	Δx mm	Δy mm
$Q = 0$	1–16	0–0.01	10–150	70–280	0–2
$Q > 0$	0–9	0.001–1	20–3 000	80–220	13–50

($h << W$) of constant cross-section with slightly non-parallel walls. Under these limitations, the developed velocity field of the free-particle flow for a channel of trapezoidal cross-section with linear lateral change of the local depth h,

$$h = h(y) = h_0 + y \operatorname{tg} \alpha \ , \tag{3}$$

can be found in the localized form: $v_x(y,z) = v_m[h(y)][1 - (2z/h(y) - 1)^2]$, where

$$v_m = v_m(h) = \frac{6Q}{W(h_0 + h_1)(h_0^2 + h_1^2)} h^2 \ . \tag{4}$$

Let us assume, in addition, that the observed particle moves strictly in the plane of channel symmetry. The corresponding unambiguous quasi-steady local characterization of the particle motion (*i.e.*, with neglected effects of both the particle own inertia and the global cross-section parameters h_0, h_1, W) consists of the following set of seven operation parameters:

$$\{h, \alpha, v_m; \rho, \nu; \pi(\rho_p - \rho)g_x d^3/6, d\}$$

which can be grouped into the four independent similarity criteria (see Symbols):

$$\{\lambda, Ar, \operatorname{tg} \alpha, Re_m\}.$$

The components, $U_x = U_x(y)$ and $U_y = U_y(y)$, of local migration velocity are dependent quantities, which can be correlated in the form like $U_x/U_\infty = f(\lambda, Ar, \operatorname{tg} \alpha, Re_m)$, *etc*. Development of the corresponding correlation equations based on the obtained experimental data for the low-Re region of motion, $Ar < 500$, is the actual task for the following sections.

RESULTS

Settling Velocities at Q = 0

The experiments under zero flow rate were conducted in the same vertical narrow channels with non-parallel walls (see Table I) as used in the experiments with $Q > 0$. The overall experimental procedure is the same as described in the previous sections. The primary data treatment consists in selecting the linear part of the sequence $x_i = x_i(t_i)$ and determining a smoothed estimate of $U_0 = \mathrm{d}x/\mathrm{d}t$ by linear regression. The obtained data on the settling velocities U_0 were correlated in the form $U_0/U_\infty = \chi(\lambda, Ar)$ using the semiempirical formula

$$\chi = 1 - 1.004\,\lambda + 0.418\,\lambda^3 - 0.169\,\lambda^5 - 0.245\,\lambda^7 + \frac{\sqrt{Ar}}{100 + 2\sqrt{Ar}}(\lambda - \lambda^7) \ , \tag{5}$$

where the terminal settling velocities U_∞ were taken from Eq. (*1*). The formula (*5*) reduces to the form suggested by Faxén[6] when setting $Ar = 0$ and neglecting the terms $O(\lambda^7)$. The agreement of this formula with the available data for $Ar < 500$, both from the present experiments and from literature, is illustrated in Fig. 3. Clusters of the points of the same kind represent single experimental runs, changes of λ within a single run are caused by a slight lateral migration. Note that the formula referred to in ref.[7] (see Eqs (*7–4.27*), p. 327) fails in the region of $\lambda > 0.5$.

Longitudinal Migration at Q > 0

When determining the longitudinal and lateral velocity components under a non-zero flow rate, the primary data on $x = x(t)$, $y = y(t)$ were first smoothed by fitting to the third-order polynomial and then differentiated to provide the experimental dependencies $U_x = U_x(h)$, $U_y = U_y(h)$.

For very small values of $\lambda = d/h$, a small particle in the symmetry plane of channel could move in a similar way as a single particle in a large volume of moving liquid. It moves vertically with respect to the local fluid velocity (in the symmetry plane of channel). The resulting vertical particle velocity for an external observer is $U_x = U_\infty + v_m$. For a larger λ, the settling velocity U_∞ in this formula could be replaced by U_0 and superposed with a fraction, $\psi = \psi(\lambda, Ar, Re_m)$, of the maximum flow velocity v_m: $U_x = U_0 + \psi v_m$. Starting with these considerations, the following correlation scheme was suggested: $(U_x - U_0)/v_m = \psi(Ar, \lambda, Re_m)$. The final correlation,

$$\Psi = \begin{cases} 1 & ; \lambda < \lambda_0 \\ \left(1 + \frac{2}{3}\frac{\lambda - \lambda_0}{1 - \lambda_0}\right)\left(\frac{1-\lambda}{1-\lambda_0}\right)^{2/3} & ; \lambda > \lambda_0 \end{cases}, \qquad (6)$$

where λ_0 depends on Ar,

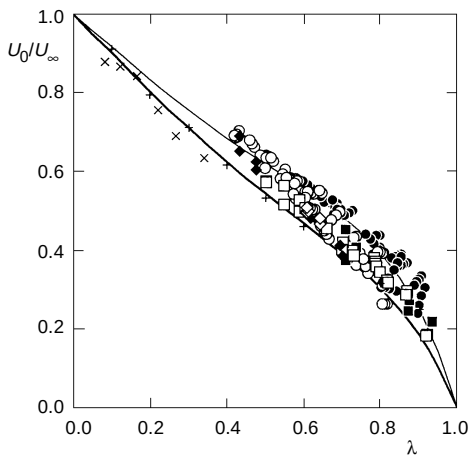

FIG. 3
Data on settling velocities. *Ar* values: 400–500 (●), 200–300 (❍), 45 (■), 20–30 (❒), 12 (◆), 2 (✧); ref.[9] (+), ref.[10] (×); Eq. (*5*), $Ar = 500$ (———); Eq. (*5*), $Ar = 0$ (▬▬)

$$\lambda_0 = \frac{0.5}{[1 + (Ar/200)^2]} \ , \qquad (7)$$

is compared with the experimental data in Fig. 4. Here, U_x are the primary data, U_0 are calculated from the operation parameters according to Eq. (*5*) and h, v_m are calculated from Eqs (*3*) and (*4*).

Lateral Migration

According to underlying theories (see, *e.g.*, ref.[8]), the lateral migration in our experiments should be an inertia effect which asymptotically disappears for $Ar \to 0$. Preliminary trials to correlate the data on lateral migration velocities resulted in the following correlation formula

$$U_y = K\,\Omega_m\, d\, Re_0 \ , \qquad (8)$$

where Ω_m is the vorticity of flow in the centre plane of the channel,

$$\Omega_m = \frac{dv_m}{dy} = \frac{2v_m}{h} \operatorname{tg} \alpha \ , \qquad (9)$$

and $K = K(Ar, \lambda, Re_m, \operatorname{tg}\alpha)$ is an unknown function. The data presented in Fig. 5 support the hypothesis that K is almost constant over a wide range of operating parameters Ar, λ, Re_m. Due to the large dispersion of primary data in Fig. 5, the result cannot be better than merely an order-of-magnitude estimate,

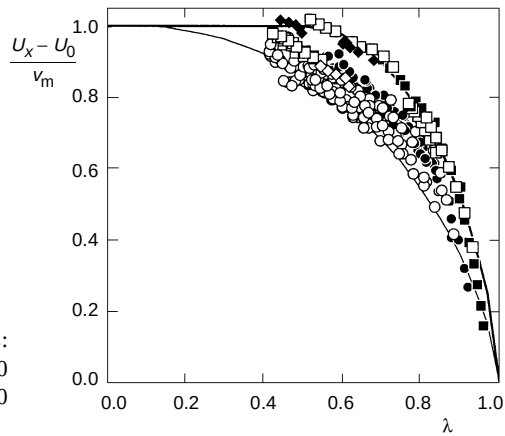

FIG. 4
Data on longitudinal migration. *Ar* values: 400–500 (●), 200–300 (○), 45 (■), 20–30 (□), 12 (◆), 2 (◇); Eq. (*6*), Ar = 500 (———); Eq. (*6*), *Ar* = 0 (▬▬)

$$K \approx 0.1 \ . \qquad (10)$$

Note that Eq. (*8*) can be written in the form $U_y/U_0 = (2K\ \lambda^2\ \mathrm{tg}\ \alpha)Re_m$. The proportionality $U_y/U_0 \approx Re_m$ indicates an inertial mechanism of the lateral migration.

A quantitative study of this effect will need an essential improvement of experimental technique, in particular: more regular and well-centered spherical particles, a longer channel, and a visualization technique with higher graphical resolution.

CONCLUSIONS

Using a visualization method, three-dimensional quasi-steady low-*Re* (*i.e.*, low-*Ar*) motion of spherical particles in Newtonian liquids flowing through a narrow vertical channel with non-parallel walls was studied which exhibits strong longitudinal and lateral migration.

The settling velocities in a Helle–Shaw cell with non-parallel walls under no flow conditions, U_0, were successfully correlated using Eq. (*5*). The inertia effects, represented by *Ar*, are included both in this formula and in Eq. (*1*) for the terminal settling velocity U_∞. The results for small but finite *Ar* are slightly higher in comparison with the data according to refs[9,10].

It seems that data on the longitudinal migration velocities U_x in a liquid flowing through a narrow channel, $Q > 0$, are reported for the first time. The correlation according to Eq. (*6*) fits the data fairly well, including the slight inertia effects (non-zero *Ar*). The main source of minor discrepancies in the *Ar*-dependent trends of ψ is probably an inaccurate smoothed estimate of U_0 which is critically sensitive to the determination of

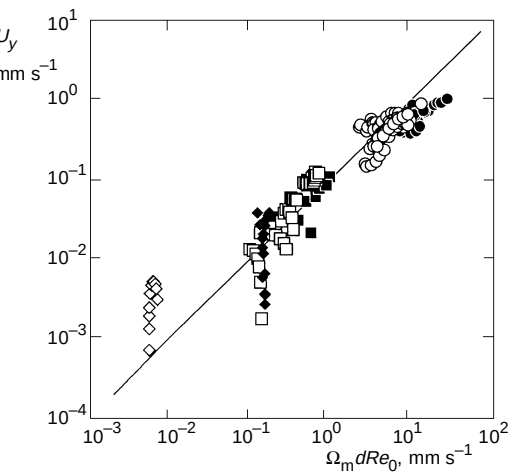

FIG. 5
Data on lateral migration. *Ar* values: 400–500 (●), 200–300 (○), 45 (■), 20–30 (❐), 12 (◆), 2 (✧); Eq. (*8*) (———)

the density difference. Note that the resulting ψ-factor is calculated by subtracting two quantities, U_x and U_0, determined with some errors.

The original observations of the lateral migration, driven by the lateral gradient of liquid velocity, Ω_m, were correlated using the settling velocities under zero flow-rate conditions, U_0. The correlation scheme (see Eq. (*8*) and Fig. 5) indicates an inertial mechanism of this motion. The hypothesis $K(\lambda, Ar, Re_m)$ = const. should be further checked as it is based on the data with rather narrow variations of viscosity and density differences.

SYMBOLS

Ar	$= g_x \lvert \rho_p/\rho - 1 \rvert d^3\nu^{-2}$, Archimedes number
d	particle diameter, m
g_x	= 9.81 m s^{-2}, gravity acceleration
h	$= h(y)$, variable depth of the channel with non-parallel walls, Eq. (*3*)
h_0, h_1	unequal sides of the channel, m, see Fig. 1
Q	volume flow rate of liquid, m^3 s^{-1}
Re_m	$= v_m h/\nu$, local flow Reynolds number
Re_0	$= \lvert U_0 \rvert d/\nu$, local particle Reynolds number in channel
Re_∞	$= \lvert U_{in} \rvert d/\nu$, particle Reynolds number in bulk liquid
tg α	$= (h_1 - h_0)/W$, skewness of the trapezoidal channel cross-section, see Fig. 1
t_{res}	residence time of a particle in visualized area, s
$U_0(h)$	settling velocity in channel under zero flow rate, m s^{-1}, Eq. (*5*)
$U_x(h)$	longitudinal (vertical) velocity of a particle, observed from the front view, m s^{-1}
$U_y(h)$	lateral migration velocity of a particle, observed from the front view, m s^{-1}
U_∞	terminal settling velocity of a particle in unbounded still fluid, m s^{-1}, Eq. (*1*)
$v_m(h)$	local maximum liquid velocity in channel symmetry plane, m s^{-1}, Eq. (*4*)
W	channel width, m, see Fig. 1
x	longitudinal coordinate (in the direction of gravity acceleration), m
Δx	longitudinal distance covered by the particle during t_{res}, m
y	lateral coordinate (horizontal and parallel to the channel symmetry plane), m
Δy	lateral distance covered by the particle during t_{res}, m
z	normal coordinate (orthogonal to the channel symmetry plane), m
ν	kinematic viscosity, m^2 s^{-1}
λ	$= d/h$
χ	$= U_0/U_\infty$
ψ	$= (U_x - U_0)/v_m$
ρ	liquid density, kg m^3
ρ_p	particle density, kg m^3
Ω_m	local vorticity in channel symmetry plane, s^{-1}, Eq. (*9*)

This work was supported by the Grant Agency of the Czech Republic (Grant No. 104/93/2285). We are grateful to Prof. V. Sobolik for his help in designing the Helle–Shaw cell.

REFERENCES

1. Feng J., Hu H. H., Joseph D. D.: *J. Fluid Mech.* **1994**, *277*, 271.
2. Nirschl H., Dwyer H. A., Denk V.: *J. Fluid Mech.* **1995**, *283*, 273.
3. Jeffrey R. C., Pearson J. R. A.: *J. Fluid Mech.* **1995**, *22*, 721.
4. Brenner H.: *Adv. Chem. Eng.* **1966**, *6*, 287.
5. Brauer H.: *Grundlagen der Einphasen- und Mehrphasenströmungen*. Verlag Sauerlander, Aarau 1971.
6. Faxen H.: *Ann. Phys. (Leipzig)* **1922**, *68*, 89.
7. Happel J., Brenner H.: *Low Reynolds Number Hydrodynamics*. Prentice Hall, Englewood Cliffs, NJ 1965.
8. Leal L. G.: *Annu. Rev. Fluid Mech.* **1980**, *12*, 435.
9. Miyamura A., Iwasaki S., Ishii T.: *Int. J. Multiphase Flow* **1981**, *7*, 41.
10. Machac I., Lecjaks Z.: *Chem. Eng. Sci.* **1995**, *50*, 143.